GNSS Independent Random Access Schemes for Beam Hopping Satellite Systems

Marius Caus*, Xavier Artiga*, Musbah Shaat*, Alessandro Guidotti†
*Centre Tecnològic de Telecomunicacions de Catalunya-CERCA (CTTC-CERCA), Castelldefels, Barcelona, Spain
†National Inter-University Consortium for Telecommunications (CNIT), Parma, Italy

***Abstract*—This paper investigates the application of the random access procedure (RAP) to beam hopping satellite systems. Furthermore, modifications are proposed to support global navigation satellite systems (GNSS) independent operation in low Earth orbit (LEO) constellations. In such a case, the time and frequency offsets that stem from the orbital motion are not perfectly compensated during the RAP. To handle the residual errors, the pre-compensation mechanism and the physical random access channel (PRACH) have been modified. The experimental validation shows that the solution described in this work enables to realize the first step of the RAP in presence of user equipment (UE) positioning errors.**

I. Introduction

With the advent of the 5G non-terrestrial network (NTN) component, 5G and satellite connectivity become instrumental to cover un-/underserved areas. This is the case for remote rural regions and maritime scenarios, where the deployment of terrestrial infrastructures is not feasible due to technical and economic reasons. Remarkably, there are several applications that could benefit from ubiquitous connectivity and low-latency communications. Some examples include safe operation of autonomous vehicles and provision of health care service remotely. To support these services, low-Earth orbit (LEO) satellite constellations step in to provide low-latency communications.

It shall be emphasized that there has been a remarkable standardization effort in Release 17 to include NTN into the 3GPP ecosystem. In this release, two satellite operating bands are included in the frequency range 1 (FR1). Concerning the architecture, only transparent payloads are specified. The normative work has included adaptations to the protocol to handle long round trip time (RTT) delays and large Doppler frequency shifts. Within the scope of the radio access network (RAN), Release 18 introduced enhancements that are detailed in [1]. The most remarkable one is the identification of additional spectrum in the Ka band for NTN. As part of Release 19, a new work item is proposed in [2] to define further enhancements for NTN, e.g., support to beam hopping and NTN architectures with regenerative payload.

Taking into consideration the upcoming features of NTN, one of the objectives of this work is to investigate the impact of applying beam hopping on the 5G protocol. As a first step, we have focused on analyzing the interplay between the beam illumination pattern and the random access procedure (RAP).

Within the scope of the RAP, the second objective of this paper is to challenge the assumptions made in the standard. The approach that is followed by 3GPP involves an open loop mechanism where the UE autonomously pre-compensates for the instantaneous RTT delay and the Doppler effects of the satellite service link. This is achieved by leveraging the global navigation satellite systems (GNSS) information, along with the satellite ephemeris information, which is broadcasted as system information. In the case of positioning errors, as in the GNSS independent operation, the UE will not be able to accurately compensate the time and frequency misalignment that originate from the orbital motion. In such a case, the resulting time offset (TO) and carrier frequency offset (CFO) may exceed the values tolerated by the standard, which call for new ideas. To deal with this aspect, this work thoroughly reviews the RAP and proposes modifications that are capable of absorbing the uncertainties. This involves the time advance mechanism and the physical random access channel (PRACH) signal design and detection.

To make the RAP more robust to imperfect pre-compensation, several preamble formats have been proposed in the literature in order to handle large TO and CFO values, e.g, [3]–[5]. The preamble structure in [3], [4], is based on concatenating a single root Zadoff-Chu (ZC) sequence with various cyclic shifts. The detector proposed in [3] individually detects each sequence to determine the presence of the preamble. The performance of this scheme is improved in [4], where all the sequences are jointly processed, by means of a non-coherent accumulation. However, to find a pattern, a sliding window detection method shall be implemented. Since the windows are partially overlapped, the downside risk associated is that the preamble could be detected in multiple windows. To resolve the ambiguity, additional conditions need to be evaluated, which increased the complexity. Another well-suited preamble is obtained by concatenating multiple different root ZC sequences [5]. Despite this solution achieves the highest robustness to the CFO, it comes at the cost of using multiple root ZC sequences to generate each candidate. Thus, making a less efficient use of resources than [3] and [4].

The preamble design that is conceived in this paper is obtained by cascading multiple identical ZC sequences. Thus, a single root ZC sequence is employed for each candidate, which is aligned with the preamble generation method described in the standard. The enhancement with respect to the standardized RAP, stems from the possibility of estimating much longer delays. Concerning the detector, analogously to [4], we reap the benefits of jointly processing multiple sequences to improve

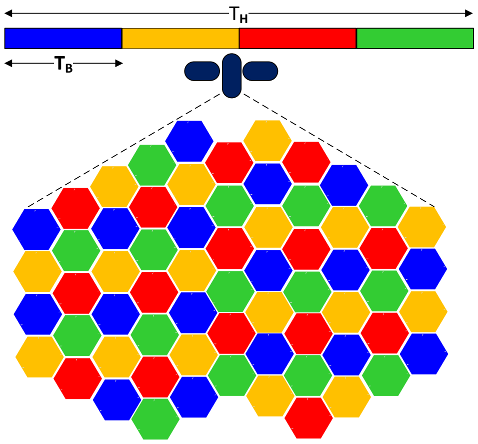

Fig. 1: An example of hopping pattern and illumination period.

the performance. Unlike [4], the detection window is fixed, so that ambiguities do not occur in the detection. Numerical results show that successful preamble detection is achieved in low Earth orbit (LEO) satellite systems that operate at the Ka band with imperfect user equipment (UE) positioning.

The rest of the paper is organized as follows. In Section II, we define the scenario. The PRACH signal detection is described in III. In Section IV, we provide design guidelines for a robust PRACH format. The numerical results are provided in Section V. Finally, Section VI draws the conclusions.

II. Scenario Definition

In the scenario under study the coverage area is divided into multiple beams. To smooth the application of 5G to NTN, priority is given to Earth-fixed beams, so that an analogy can be drawn with terrestrial deployments. In this work, we focus on LEO satellite systems with regenerative capabilities. Owing to power limitations, it is assumed that satellites are not able to simultaneously illuminate all the beams in the field of view (FoV). As a result, the implementation of beam hopping solutions is required, which has a profound effect in several procedures. In this work, we give emphasis to the initial step of the RAP, where the gNB shall detect the PRACH signals. To this end, the UEs that request access to the network use a set of configured random access resources. The standard supports one-to-one, one-to-many and many-to-one association between the beams and the random access resources. This means that the resources available for the PRACH signal reception can be shared by multiple beams or alternatively, it is possible to establish a one-to-one relation between beams and resources.

The periodicity of the random access resources is a configurable parameter that is specified in the standard to control the random access latency. Since the satellite is not able to simultaneously illuminate all the directions, the network shall choose the PRACH periodicity T_{PRACH} according to the hopping period T_H, which is the time required to illuminate all the directions. In the random access context, the beam hopping technique is not driven by the traffic but shall be designed to periodically sweep all the spots in the FoV.

TABLE I: System and orbit parameters

Parameter	Value
Inclination	50°
Altitude	1300 km
Beam radius	50 km
Number of Planes	20
Satellites per Plane	11
Total number of satellites	220
Minimum elevation angle	30°
Frequency band	Ka

Assuming that the beams can be redirected every T_B seconds, the hopping period can be expressed as $T_H = R_B T_B$, where R_B is the ratio of the total number of beams to the number of simultaneously illuminated beams. In the case represented in Figure 1, the beam illumination pattern is particularized for $R_B = 4$. At a given slot, the active beams are not adjacent to reduce co-channel interference. The PRACH configuration specified in [6] allows the network to set $T_{\text{PRACH}} = \{10, 20, 40, 80, 160\}$ ms. The requirement to apply the standardized RAP to beam hopping satellite systems schemes relies on the fulfilment of this inequality $T_H \leq 160$ ms. The satellite payload defined in [7] highlights that analog and hybrid beamforming architectures cannot meet this requirement. To overcome this issue, higher random access latency values should be specified. This motivates the use of digital beamforming architectures, which allow reducing the beam switching rate.

III. PRACH signal detection

This section analyses the PRACH signal detection in LEO satellite systems. The main impairments include the long RTT delay and the Doppler frequency shift. The UE is able to autonomously compensate these effects, by using its positioning functionality as well as the satellite ephemeris.

Concerning the UE position, this work departs from the standardized GNSS-assisted pre-compensation solution. Alternatively, it relies on a GNSS independent method where the UE positioning information is obtained by tracking the reference signals transmitted by LEO satellites. The synchronization signal block (SSB) exemplifies a signal of opportunity for positioning [8]. When a single satellite is visible, the positioning error could be in the order of km. In such a case, the UE is not endowed with the ability to perfectly pre-compensate the instantaneous Doppler effects and the RTT delay on the service link. The rest of the section is devoted to assess the impact that the resulting TO and CFO has on the RAP.

The system and orbit parameters that are considered in this work are gathered in Table I. The values have been obtained from the reference constellation designed in [7].

A. Carrier frequency offset

In alignment with the PRACH performance evaluation carried out in [9], the maximum uplink CFO associated with the

TABLE II: Uplink CFO for LEO 1300km

Ka-band for $R_\epsilon = 5$km		
Scenario	Vehicular at $\theta = 30°$	Vehicular at $\theta = 90°$
CFO (KHz)	± 18.1	± 8.2

TABLE III: Uplink TO for LEO 1300km

Ka-band for $R_\epsilon = 5$km		
Scenario	Vehicular at $\theta = 30°$	Vehicular at $\theta = 90°$
TO (μs)	± 29	± 0.07

PRACH signal detection can be expressed as

$$\begin{aligned} CFO_{UL} = \; & \left(DS_{RO} \times 10^{-6} + DS_{UE} \times 10^{-6} + 1\right)^2 \times \\ & \left(f_{RO} \times 10^{-6} + 1\right) \times f_c^{UL} - f_c^{UL}, \end{aligned} \tag{1}$$

where f_c^{UL} is the carrier frequency in the uplink and f_{RO} denotes the residual frequency offset after the downlink synchronization in ppm. As it is specified in [10], the UE modulated carrier frequency should be accurate to within $f_{RO} = \pm 0.1$ppm. The Doppler frequency shift due to UE movement is represented by DS_{UE}. To support the vehicular use case, we have considered speeds up to 250 km/h. In the absence of GNSS information, the UE is not able to adjust the carrier frequency to counteract the Doppler effects. To this end, we involve the residual Doppler frequency shift DS_{RO} in the analysis. The imperfect compensation stems from the inaccuracies in the UE position. Following the guidelines reported in [4], we have computed the maximum DS_{RO} as function of the uncertainty range R_ϵ.

In Table II, we provide the maximum CFO for different elevation angles θ. Note that the highest mismatch of the uplink frequency is observed at $\theta = 30°$, where the Doppler induced by the terminal mobility is the highest.

B. Time offset

In the proposed mode of operation, the PRACH signal will be misaligned in time domain due the imperfect UE positioning. Large TO values are observed at low elevation angles. For an uncertainty region of radius $R_\epsilon = 5$km, the highest residual TO values are provided in Table III. Analogously to Section III-A, we have used the parameters defined in Table I. Furthermore, we have followed the guidelines reported in [4] to compute the differential RTT delay between two positions.

C. Analysis of 5G NR preamble formats

The objective of this section is to analyse the robustness of the preamble formats specified in [6] to deal with time and frequency offsets. The most suitable designs for NTN correspond to the formats B4 and C2. This is because the repetition scheme that is used to generate the format B4 allows detecting the preamble in low signal-to-noise ratio (SNR) conditions. The cyclic prefix (CP) transmitted by the format C2 is useful to support long delays. The rest of formats either transmit a shorter CP or less repetitions. Hence, they are more vulnerable to the TO and more sensitive to noise and interference than the formats C2 and B4, respectively.

TABLE IV: Tolerance to time offsets supported by preamble formats B4 and C2

Preamble formats	B4			
SCS (KHz)	15	30	60	120
TO (μs)	30.47	15.23	7.61	3.80
Preamble formats	C2			
SCS (KHz)	15	30	60	120
TO (μs)	66.67	33.34	16.67	8.33

The preamble format B4 is generated by concatenating 12 ZC sequences, while the format C2 consists of 4 ZC sequences. The CP duration in B4 and C2 formats is, respectively given by $T_{CP} = 30.47 \times 2^{-\mu}\mu s$ and $T_{CP} = 66.66 \times 2^{-\mu}\mu s$. Remarkably, the variable μ controls the subcarrier spacing (SCS) as $\Delta_f = 15 \times 2^\mu$ kHz.

In Table IV, we present the TO that is tolerated by the formats B4 and C2, for different SCS. To ensure successful preamble detection two conditions shall be satisfied, namely: the TO shall be lower than the CP duration; the CFO shall not exceed half the SCS. If these conditions are not met, it is not possible to separate the two effects, i.e., delay and frequency shifts, leading to timing ambiguities. By closely analysing the maximum TO and CFO values computed in Sections III-A and III-B, we can resolve that enhancements are required to operate in the absence of GNSS. It shall be noted that an uncertainty range of $R_\epsilon = 5$km, is consistent with the accuracy that can be achieved with a single LEO satellite [8].

IV. Design guidelines for a robust PRACH format

In presence of UE position inaccuracies, the pre-compensated Doppler frequency and RTT delay will be subject to errors. This section provides some design guidelines to mitigate the impact of these errors on the RAP.

A. Timing advance pre-compensation method

Imperfect compensation will lead to either underestimated or overestimated RTT delay. Consequently, the PRACH signal could be delayed or received in advance with respect to the random access occasion. This is shown in Figure 2. The time misalignment may lead to interference to already synchronized signals. The delays can potentially be absorbed by the guard interval (GI). However, when the PRACH signal reception is affected by negative offsets, previous slots cannot be protected. To overcome the effects from overestimating the RTT delay, the transmission timing of the PRACH signal has to be delayed according to the maximum estimation error made by the UE. Then, the time advance (TA) that shall be applied for the transmission of the preamble is given by

$$\begin{aligned} T_{\text{TA}} = T_C \Big(& N_{\text{TA}} + N_{\text{TA,offset}} + N_{\text{TA,adj}}^{\text{common}} + \\ & N_{\text{TA,adj}}^{\text{UE}} - N_{\text{TA,margin}} \Big), \end{aligned} \tag{2}$$

where $N_{\text{TA,margin}}$ is a new configurable parameter used as a margin to handle the uncertainty and $T_C = 1/(480000 \times 4096)$s is the basic time unit in the specifications. The rest of the parameters are inherited from the legacy TA mechanism, as specified in [6], [11].

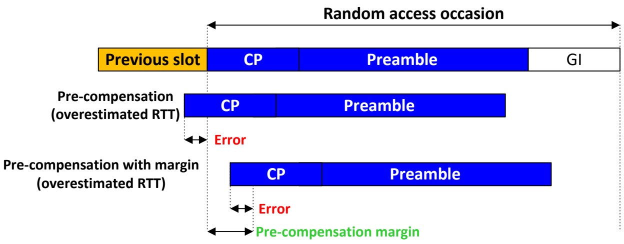

Fig. 2: Pre-compensation with and without margin when the RTT delay is overestimated.

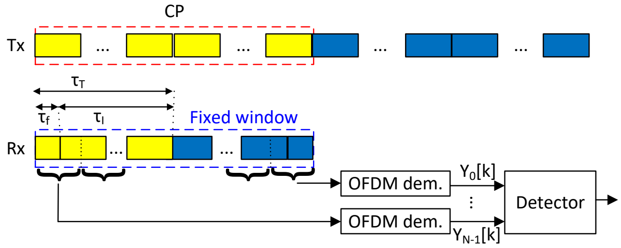

Fig. 3: The detection window for the fractional delay.

It is noteworthy to mentioning that if the uncertainty is within $[-T_C N_{\text{TA,margin}},\ T_{\text{CP}} - T_C N_{\text{TA,margin}}]$, then it follows that the network will be able to handle overestimated and underestimated delays with unipolar commands. The concept is illustrated in Figure 2. In notation terms, the variable that represents the equivalent delay upon applying the margin $N_{\text{TA,margin}}$, is defined by TO_{UL}.

B. PRACH signal design and system model

The PRACH configuration is another aspect that can be enhanced to increase the robustness to TO. The frequency range 2 (FR2) NTN configuration drafted in [12] will be used as baseline. To increase the capability to handle positioning errors, we propose to extend the GI beyond the values supported by the 3GPP. This comes at the cost of reducing the number of random access occasions and hence, the PRACH capacity as well. In exchange, the reliability of GNSS indepedent random access schemes is enhanced.

To generate the novel PRACH signal, the preamble is obtained by concatenating $N+N_{CP}$ identical ZC sequences. The resulting signal is fed into the multicarrier modulator, which implements the discrete Fourier transform spread orthogonal frequency division multiplexing (DFT-s-OFDM) waveform. At reception, due to the imperfect compensation, the PRACH signal is delayed and frequency shifted by TO_{UL} and CFO_{UL}, respectively.

As Figure 3 shows, the delay can be expressed in samples as $\tau_T = TO_{UL} \times f_s = \tau_f + \tau_I$. The sampling frequency is set to $f_s = \Delta_f M$, where M denotes the number of subcarriers. The fractional and the integer delays are expressed as $\tau_f = \text{mod}\,(\tau_T, M)$ and $\tau_I = M\lfloor \tau_T/M \rfloor$. At reception, the first N_{CP} symbols are discarded. If N_{CP} is dimensioned according to the maximum delay, the gNB can use a fixed detection window to capture N symbols. Then, the samples are divided into N sequences that are processed by the OFDM demodulator. Adopting the system model applied in [13], the j-th demodulated sequence is represented in the frequency domain by

$$Y_j[k] = h \times D_M\left(\epsilon_f\right) X_u[k] e^{-j\frac{2\pi}{M}\tau_f k} + W_j[k] + I[K], \quad (3)$$

for $j = 0, \cdots, N-1$ and $k = 0, \cdots, N_{\text{ZC}}-1$. The transmitted signal $X_u[k]$ is the frequency domain representation of the time-domain ZC sequence $x_u[n] = e^{-j\frac{\pi u n(n+1)}{N_{\text{ZC}}}}$, which is defined for $0 \leq n \leq N_{\text{ZC}} - 1$. Accordingly, we get

$$X_u[k] = \frac{1}{\sqrt{N_{\text{ZC}}}} \sum_{n=0}^{N_{\text{ZC}}-1} x_u[n] e^{-j\frac{2\pi}{N_{\text{ZC}}}kn}. \quad (4)$$

The preamble is characterized by the root index u. Interestingly, τ_f translates into a phase rotation, thanks to the circular structure of the PRACH signal. From the series

$$D_M(x) = \frac{1}{M} \sum_{n=0}^{M-1} e^{j\frac{2\pi}{M}xn}, \quad (5)$$

we can characterize the impact of the CFO evaluated on the radial frequency $\omega = 2\pi\epsilon_f/M$, where $\epsilon_f = CFO_{UL}/\Delta_f$. It is assumed that $|\epsilon_f| < 0.5$. Equation (3) reveals that the CFO affects the amplitude of the signal and induces inter-carrier interference (ICI), which is formulated as

$$I[k] = h \times e^{-j\frac{2\pi}{M}\tau_f k} \sum_{\substack{i=0 \\ i\neq k}}^{N_{\text{ZC}}-1} D_M\left(\epsilon_f + i - k\right) X_u[i]. \quad (6)$$

As for the propagation conditions, the line of sight (LoS) channel h has been formulated as function of the typical antenna gains and propagation losses. For the sake of brevity we do not include the closed-form expression. The details can be found in [4]. One aspect that is important to remark is that the channel is normalized to the power spectral density of the noise at the input of the receiver. Hence, the noise samples are independent and identically distributed as $W_j[k] \sim \mathcal{CN}\left(0, 1\right)$.

C. Delay estimation

To estimate the fractional delay, the detector computes the correlation

$$\rho_{\nu m} = \sum_{j=0}^{N-1} \left| \sum_{k=0}^{N_{\text{ZC}}-1} Y_j[k] X_\nu^*[k] e^{j\frac{2\pi}{N_{\text{FFT}}}mk} \right|^2, \quad (7)$$

for $0 \leq m \leq N_{\text{FFT}} - 1$. The variable N_{FFT} controls the resolution of the estimated delays. To enhance the detection, the decision variable is computed by performing a non-coherent accumulation. Note that in (7) only a subset of N out of $N + N_{CP}$ symbols is used to get an estimate of τ_f. If the locally generated preamble coincides with the transmitted preamble, then (7) will exhibit a correlation peak

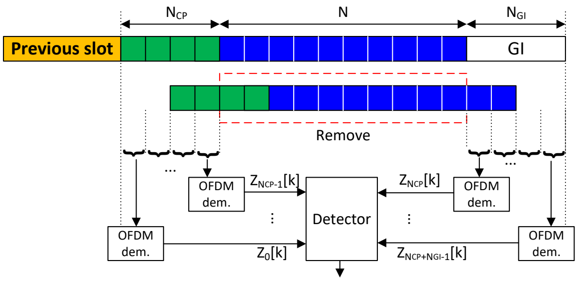

Fig. 4: The detection window for the integer delay.

at $(\nu, m) = \left(u, \lceil \frac{N_{\text{FFT}}}{M}\tau_f \rceil\right)$. It is worth emphasizing that only the correlation values that exceed a predefined threshold are classified as peak values. The peak search is executed in the subset that satisfies $\rho_{\nu m} \geq r_{\text{th}}$. The threshold is fully characterized by the chi-square distribution with N degrees of freedom and the target false alarm probability, [3], [14]. From the peak position, it is straightforward to estimating the fractional delay. However, the detector is not able to find the boundaries of the PRACH signal, leading to estimation errors. This observation highlights that new detection strategies shall be devised to estimate the integer part of the delay. Some insights are provided in the following paragraphs.

Once the fractional part of differential delay is obtained, the received PRACH signal can be shifted back τ_f samples, so that the symbol boundaries are aligned with the reference of the PRACH slot. The estimation of τ_I is equivalent to determining the beginning of the PRACH signal. As Figure 4 highlights, the idea is to remove the symbols that have been used to detect the fractional delay and then, find the boundaries of the received burst from the demodulated sequences $\{Z_0[k], \cdots, Z_{N_{CP}+N_{GI}-1}[k]\}$. This can be accomplished by computing the cross-correlation measurement

$$R_l = \sum_{i=l}^{l+N_{CP}-1} R_{Z_i X}, \tag{8}$$

with $0 \leq l \leq N_{GI}$ and

$$R_{Z_i X} = \left| \sum_{k=0}^{N_{\text{ZC}}-1} Z_i[k] X_u^*[k] \right|^2. \tag{9}$$

Without loss of generality, it is assumed that the GI encompass N_{GI} OFDM symbols. The sequence $Z_i[k]$ either integrates a complete frequency-domain ZC sequence or just contains noise and interference. When the signal is present, $R_{Z_i X}$ corresponds to a correlation peak. However, this only holds true if the estimated fractional delay $\hat{\tau}_f$ is sufficiently accurate. Problems arise when the estimation error is close to $\frac{1}{N_{\text{ZC}}\Delta_f}$. In such a case, there could be a drop in the value of $R_{Z_i X}$. To ensure that $R_{Z_i X}$ does not drop in value for small fractional delay estimation errors, we recast (9) as

$$R_{Z_i X} = \left| \sum_{k=0}^{N_{\text{ZC}}-1} Z_i[k] X_u^*[k] \left(\sum_{t=-1}^{1} e^{j\frac{2\pi}{N_{\text{ZC}}}0.5kt} \right) \right|^2. \tag{10}$$

TABLE V: PRACH configuration.

PRACH bandwidth	B_{PRACH}=8.34MHz
PRACH subcarrier spacing	$\Delta_f = 60$ KHz
Size of the ZC sequence	$N_{\text{ZC}} = 139$
Number of subcarriers	$M = 256$
FFT size of the detector	$N_{\text{FFT}} = 256$
Length of the preamble	$N_{CP} = N = 4$ symbols
Length of the GI	$N_{GI} = 4$ symbols

With this modification, we increase the chance to identify the peak. The main reason is because (10) accumulates the correlation values at $\hat{\tau}_f$ as well as $\hat{\tau}_f \pm \frac{0.5}{N_{\text{ZC}}\Delta_f}$. However, it deserves to be mentioned that the sensitivity to the estimation error is increased at the cost of enhancing the noise. This can be mitigated by performing three parallel correlations and taking the maximum. It becomes evident that this method entails a complexity increase. Regardless of the cost function that is used to compute $R_{Z_i X}$, the integer delay will be determined as follows

$$\hat{\tau}_I = \underset{0 \leq l \leq N_{GI}-1}{\text{argmax}} \ R_l. \tag{11}$$

V. Numerical Results

The performance of the proposed design is evaluated using the orbit and the system parameters described in Table I. The PRACH configuration is provided in Table V. To support the modified preamble format, the random access occasion shall span at least 12 OFDM symbols. This observation highlights that the random access configuration originally conceived for the preamble format B4, could be reused to increase the resilience to the TO.

It is assumed the UE positioning error is uniformly distributed inside a circular uncertainty region of radius $R_\epsilon = 5$ km. Concerning the channel model, LoS conditions have been assumed. Under such assumptions, the corresponding offsets are provided in Tables II and III. To compensate negative time offsets, the UE applies a pre-compensation margin of $33.3\mu s$ $\left(\frac{N_{CP}}{2}\text{samples}\right)$. Including this margin, the range of TO_{UL} is $[4.4, 62.2]\,\mu s$, for $\theta = 30°$. With $\theta = 90°$, the TO can be assumed constant and thus, $TO_{UL} = 33.3\mu s$. It can be readily verified that the preamble design specified in Table V is able to handle delays up to 66.66 μs and CFO values in the range $[-30, 30]$ KHz. Hence, the TO and the CFO that result from a positioning error of $R_\epsilon = 5$ km are within the supported ranges.

In Figures 5 and 6, the missed detection probability (MDP) is illustrated for different elevation angles. Note that three detectors are compared. Remarkably, the metric formulated in (7) is used across the three schemes to estimate the fractional delay. When the fractional delay is assumed to be perfectly estimated, the estimation of the integer delay is governed by the cross-correlation defined in (9). This detector is identified with the acronym CC. Alternatively, the detector could be governed by (10), to mitigate the impact of the imperfect fractional delay estimation. This scheme is referred to as robust CC. To determine how far the proposed detectors perform from

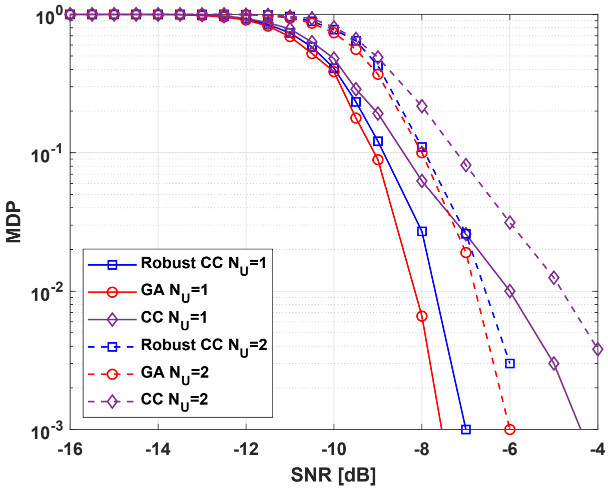

Fig. 5: MDP vs SNR for $\theta = 30°$.

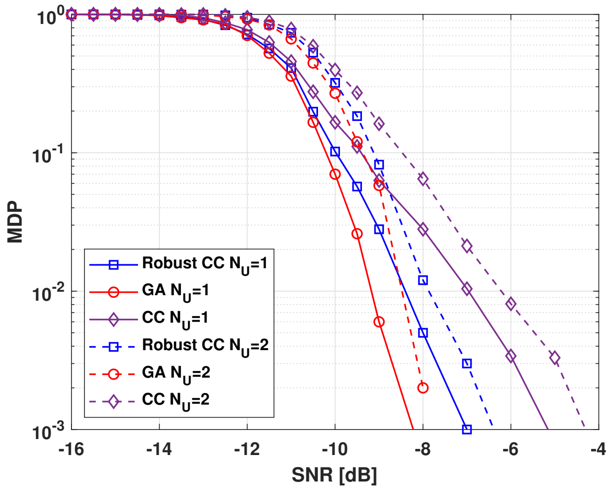

Fig. 6: MDP vs SNR for $\theta = 90°$.

the optimal solution, we have evaluated a genie-aided (GA) scheme with perfect integer delay information.

The error cases resulting in incorrect detection encompass: 1) detecting a preamble different from the one transmitted, 2) failing to detect any preamble at all, and 3) correctly detecting the preamble but with an erroneous timing estimation. Specifically, a timing estimation error is declared if the magnitude of the error exceeds $\frac{1}{N_{\text{ZC}}\Delta_f}$. The number of simultaneous users is denoted as N_U. We have considered that at most $N_U = 2$ users are simultaneously accessing the network in a single random access occasion. The same baseline has been established for the PRACH performance evaluation in [9]. The threshold that is used to classify the correlation values as peaks is computed to ensure a false alarm probability of $P_{\text{FA}} = 10^{-3}$.

The simulation verifies that the robust CC design is able to estimate the delays without significant performance degradation with respect to the GA. The degradation is less than 1 dB, regardless of the scenario, as long as the MDP is in the range $\left[10^{-2}, 1\right]$. As expected, the CC technique exhibits poor performance, The main reason stems from the fact that it is very sensitive to small delay errors.

VI. Conclusions

This paper represents a first step towards supporting beam hopping and GNSS independent operation in NTN. These upcoming features have been investigated within the scope of the RAP. Nonetheless, they will have an impact on other procedures, such as the downlink synchronization, the scheduling and the radio resource management, to mention a few. To understand the extend of the modifications in the protocol stack, more in-depth research will be required in the future.

Acknowledgment

5G-STARDUST project has received funding from the Smart Networks and Services Joint Undertaking (SNS JU) under the European Union's Horizon Europe research and innovation programme under Grant Agreement No 101096573.

This work has received funding from the Swiss State Secretariat for Education, Research and Innovation (SERI).

Part of the work is funded by "Ministerio de Asuntos Económicos y Transformación Digital" and the EU-NextGenerationEU in the frameworks of the PRTP and MRR under reference TSI-063000-2021-71 and by the Spanish National projects AEI/10.13039/501100011033 SOFIA-SKY (PID2023-1473050B-C32).

References

[1] "NR NTN (Non-Terrestrial Networks) enhancements." RP-232669, 2023.

[2] "Non-Terrestrial Networks (NTN) for NR Phase 3." RP-234076, 2023.

[3] L. Zhen, H. Qin, B. Song, R. Ding, X. Du, and M. Guizani, "Random Access Preamble Design and Detection for Mobile Satellite Communication Systems," *IEEE Journal on Selected Areas in Communications*, vol. 36, no. 2, pp. 280–291, 2018.

[4] M. Caus and M. Shaat, "PRACH Signal Design and Detection for LEO Satellite Systems with Imperfect UE Positioning," in *2024 27th International Workshop on Smart Antennas (WSA)*, 2024.

[5] L. Zhen, T. Sun, G. Lu, K. Yu, and R. Ding, "Preamble Design and Detection for 5G Enabled Satellite Random Access," *IEEE Access*, vol. 8, pp. 49 873–49 884, 2020.

[6] "3GPP; Technical Specification Group Radio Access Network; NR; Physical channels and modulation; (Release 18)." 3GPP TS 38.211.

[7] Project 5G-STARDUST, "D3.2: End-to-end ground and space integrated architecture," https://www.5g-stardust.eu/.

[8] W. Wang, T. Chen, R. Ding, G. Seco-Granados, L. You, and X. Gao, "Location-Based Timing Advance Estimation for 5G Integrated LEO Satellite Communications," *IEEE Transactions on Vehicular Technology*, vol. 70, no. 6, pp. 6002–6017, 2021.

[9] "Solutions for NR to support non-terrestrial networks (NTN); (Release 16)." 3GPP TR 38.821, 2023.

[10] "3GPP; Technical Specification Group Radio Access Network; NR; User Equipment (UE) radio transmission and reception; Part 1: Range 1 Standalone (Release 18))." 3GPP TS 38.101-1.

[11] "3GPP; Technical Specification Group Radio Access Network; NR; Physical layer procedures for control; (Release 18)." 3GPP TS 38.213.

[12] "Draft CR for 38.211 on Introduction of FR2-NTN." R1-2403791.

[13] S. Sesia, I. Toufik, and M. Baker, "Random Access," in *LTE - The UMTS Long Term Evolution: From Theory to Practice*, 2011, ch. 19, pp. 371–406.

[14] M. Caus and A. I. Pérez-Neira, "FBMC-Based Random Access Signal Design and Detection for LEO Base Stations," *IEEE Transactions on Wireless Communications*, vol. 22, no. 3, pp. 2156–2170, 2023.